Computational and Mutational Analysis of Human Glutaredoxin (Thioltransferase): Probing the Molecular Basis of the Low pK_a of Cysteine 22 and Its Role in Catalysis[†,‡,§]

Shu-Chuan Jao,[||,⊥,#,▽] Susan M. English Ospina,[||,#] Anthony J. Berdis,[#] David W. Starke,[#] Carol Beth Post,[*,⊥] and John J. Mieyal[*,#,▽]

Department of Pharmacology, School of Medicine, and Department of Chemistry, Case Western Reserve University, Cleveland, Ohio 44106-4965, and Department of Medicinal Chemistry and Molecular Pharmacology, Purdue University, West Lafayette, Indiana 47907-1333

Received August 16, 2005; Revised Manuscript Received December 26, 2005

ABSTRACT: Human glutaredoxin (GRx), also known as thioltransferase, is a 12 kDa thiol-disulfide oxidoreductase that is highly selective for reduction of glutathione-containing mixed disulfides. The apparent pK_a for the active site Cys22 residue is approximately 3.5. Previously we observed that the catalytic enhancement by glutaredoxin could be ascribed fully to the difference between the pK_a of its Cys22 thiol moiety and the pK_a of the product thiol, each acting as a leaving group in the enzymatic and nonenzymatic reactions, respectively [Srinivasan et al. (1997), *Biochemistry 36*, 3199−3206]. Continuum electrostatic calculations suggest that the low pK_a of Cys22 results primarily from stabilization of the thiolate anion by a specific ion-pairing with the positively charged Lys19 residue, although hydrogen bonding interactions with Thr21 also appear to contribute. Variants of Lys19 were considered to further assess the predicted role of Lys19 on the pK_a of Cys22. The variants K19Q and K19L were generated by molecular modeling, and the pK_a value for Cys22 was calculated for each variant. For K19Q, the predicted Cys22 pK_a is 7.3, while the predicted value is 8.3 for K19L. The effects of the mutations on the interaction energy between the adducted glutathionyl moiety and GRx were roughly estimated from the van der Waals and electrostatic energies between the glutathionyl moiety and proximal protein residues in a mixed disulfide adduct of GRx and glutathione, i.e., the GRx-SSG intermediate. The values for the K19 mutants differed by only a small amount compared to those for the wild type enzyme intermediate. Together, the computational analysis predicted that the mutant enzymes would have markedly reduced catalytic rates while retaining the glutathionyl specificity displayed by the wild type enzyme. Accordingly, we constructed and characterized the K19L and K19Q mutants of two forms of the GRx enzyme. Each of the mutants retained glutathionyl specificity as predicted and displayed diminution in activity, but the decreases in activity were not to the extent predicted by the theoretical calculations. Changes in the respective Cys22-thiol pK_a values of the mutant enzymes, as shown by pH profiles for iodoacetamide inactivation of the respective enzymes, clearly revealed that the K19−C22 ion pair cannot fully account for the low pK_a of the Cys22 thiol. Additional contributions to stabilization of the Cys22 thiolate are likely donated by Thr21 and the N-terminal partial positive charge of the neighboring α-helix.

Many cellular proteins containing sulfhydryl groups are susceptible to oxidative modifications that change their biological activity (*1*, *2*). In particular a common modification under conditions of oxidative stress is formation of mixed disulfides with glutathione (protein-SSG) (*3*−*5*), and this type of modification is also considered to be a likely mechanism of regulation and signal transduction (*6*−*9*). For example, the DNA binding activity of nuclear factor 1 and the catalytic activities of HIV-1 protease and protein tyrosine phosphatase 1B are inhibited by S-glutathionylation (refs *10*, *11*, and *12*,

[†] Supported in part by grants to J.J.M: NIH Grants RO1-AG 024413 and PO1-AG15885, a grant from the Ohio Board of Regents (Pharmacological Sciences Consortium), and a Merit Review Grant from the Department of Veteran's Affairs.

[‡] The PDB file name for the reduced human glutaredoxin (thioltransferase) is 1jhb; and for its disulfide adduct with glutathione (GRx-SSG), 1b4q.

[§] This work was presented in part at the 2003 Experimental Biology Meeting [S. M. English, A. J. Berdis, S.-C. Jao, C. Post, D. W. Starke, and J. J. Mieyal, Mutational manipulation of human glutaredoxin (thioltransferase)—effect on catalysis, Experimental Biology 2003, San Diego, Abstract No. 8506]. Part of this work contributed to fulfillment of requirements for the Ph.D. degree for S.-C.J and the M.S. degree for S.M.E.O.

* To whom correspondence should be addressed. J.J.M.: Department of Pharmacology, School of Medicine, Case Western Reserve University, 2109 Adelbert Road, Cleveland, OH 44106-4965; (216)-368-3383 (phone); (216)-368-3395 (fax); jjm5@cwru.edu (e-mail). C.B.P.: Department of Medicinal Chemistry and Molecular Pharmacology, School of Pharmacy, Purdue University, West Lafayette, IN 47907; (765)-494-4519 (phone); (765)-496-1189 (fax); cbp@cc.purdue.edu (e-mail).

[||] These authors contributed equally to the generation and interpretation of the data and therefore are considered co-first authors of this article.

[⊥] Purdue University.

[#] Department of Pharmacology, School of Medicine, Case Western Reserve University.

[▽] Department of Chemistry, Case Western Reserve University.

10.1021/bi0516327 CCC: $33.50
Published on Web 03/22/2006

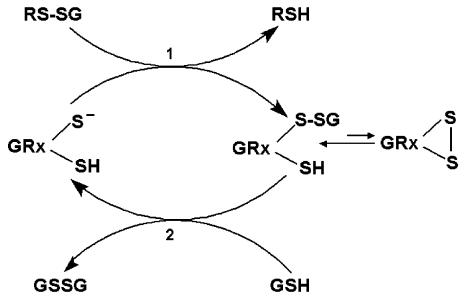

FIGURE 1: Glutaredoxin (thioltransferase) mechanism. The central portion of the scheme depicts the simple and efficient monothiol catalytic cycle for GRx. The upper left depicts nonenzymatic formation of glutathione-containing mixed disulfides which are the true substrates for GRx (*6*, *13*, *14*). The side reaction at the lower right depicts how formation of the intramolecular C22−C25 disulfide on GRx detracts from ideal catalysis (*13*, *19*).

respectively). Glutaredoxin (thioltransferase) has been characterized as a specific and efficient catalyst of protein-SSG deglutathionylation (*6*, *13*−*15*), and it is able to restore the binding activity of nuclear factor 1 (*10*) and reactivate glutathionylated PTP1B (*12*). Glutaredoxin also catalyzes the deglutathionylation of diglutathionylated HIV-1 protease in a site-specific manner at Cys95, converting the inactive enzyme to a superactive form (*11*). These and many other examples where glutaredoxin action restores function to S-glutathionylated proteins implicate the enzyme as a regulation factor in vivo (*8*, *9*, *16*).

The mechanism of glutaredoxin (GRx[1]) catalysis deduced from previous kinetics and mutagenesis studies (*6*, *13*, *14*, *17*−*19*) involves nucleophilic attack by the GRx Cys22 thiolate on the glutathionyl disulfide bond forming the GRx-SSG intermediate, followed by rate-limiting nucleophilic attack by a reduced thiol (preferentially GSH) on the GRx-SSG adduct to return reduced glutaredoxin to the catalytic cycle (Figure 1). As demonstrated (*18*), the catalytic advantage of glutaredoxin is directly attributable to the Cys22 thiolate serving as an efficient leaving group because of its low pK_a of 3.5 (*17*, *20*, *21*). The catalytic role of the Cys 22 thiolate is well accepted, but the basis for the low pK_a value is controversial. Wells et al. proposed that Arg26 or Lys27 or both are responsible for the low pK_a of Cys22 according to changes in the pH dependence of iodoacetamide inactivation of wild type and R26V and K27Q mutants of pig liver glutaredoxin (*17*). On the other hand, we and others proposed a thiol-carboxylate hydrogen bond interaction because a hydrogen bond is less affected by salt screening than an ion pair, and the pK_a of Cys22 of human and yeast glutaredoxin was not perturbed by changes in ionic strength (*20*, *21*). More recently the structure of reduced human glutaredoxin was solved by NMR (*22*), identifying the ion pair between Lys19 and Cys22. The authors suggested, however, that the low pK_a of the Cys22 thiolate was likely due to stabilization by a local positive electrostatic potential resulting from the composite local environment rather than from a single interaction. Simultaneous NMR characterization of the GRx-SSG intermediate implicated the Lys19 residue also in stabilization of the adducted glutathionyl moiety (*14*). A focus on the Lys19 residue is supported also by the occurrence of a positive side chain at that position being conserved in a broad range of glutaredoxins from multiple species (Chart 1). On the other hand, Arg 26 and Arg 27 are not conserved.

Chart 1: Sequence Alignment around the Active Site Cysteine of Various Glutaredoxins[a]

	19 22 25
GRx_Hu	VVFI**K**PT**C**PY**C**RRAQEIL
GRx_Pig	VVFI**K**PT**C**PF**C**RKTQELL
GRx_Chick	TLFV**K**GS**C**PY**C**KNAIVLL
GRx2_HuM	VIFS**K**TS**C**SY**C**TMAKKLF
GRx2_MoM	VIFS**K**TS**C**SY**C**SMAKKIF
GRx_Le	AVFS**K**TY**C**PF**C**VSVKDLL
GRx_Sc	FVAA**K**TY**C**PY**C**KATLSTL
GRx_Ec	VIFG**R**SG**C**PY**C**VRAKDLA
GRx_Vv	TIFV**K**YT**C**PF**C**RNALDIL
GRx_Hi	VIFG**R**PG**C**PY**C**VRAKNLA

[a] The alignment was produced by CLUSTALW (*38*). The sequences include GRx1 from human (GRx_Hu, P35754), pig (GRx_Pig, P12309), chicken (GRx_Chick, P79764); human GRx-2; mitochondrial precursor (GRx2_HuM, Q9NS18); mouse GRx-2; mitochondrial precursor (GRx2_MoM, Q923 × 4); tomato GRx (GRx_Le,Q9ZR41); yeast Grx-1 (GRx_Sc,P17695); *E. coli* GRx-1 (GRx_Ec, P68688); Vaccinia Virus GRx (GRx_Vv, P68692); and *H. influenzae* Grx (GRx_Hi, P45242).

We used a continuum electrostatic model to investigate the molecular basis of the low pK_a value of the Cys22 residue. This method has been used to calculate pK_a values of ionizable groups in many proteins, including BPTI, T4 lysozyme, serine proteases (*23*), DsbA (*24*), and thioredoxin (*25*). In the present study this computational approach implicated Lys19 and/or Thr21 via ion-pairing and/or hydrogen bonding interactions as the basis for the low pK_a of the active-site cysteine in human glutaredoxin. To challenge the hypothesis that the K19−C22 ion pair could be the exclusive basis for the low pK_a of the C22 thiolate, K19Q and K19L mutations of human glutaredoxin were performed in silico, and then the mutants were actually constructed, purified, and characterized kinetically. Computationally the mutants were predicted to retain specificity for glutathionyl disulfide substrates, but to have Cys22 thiol pK_a values greater than 7 and thus lose most of the catalytic activity of the WT enzyme. Empirical studies of the actual mutants confirmed retention of specificity and showed that mutation of lysine 19 does diminish the catalytic rate. However, the changes were not as large as predicted by molecular modeling, indicating important molecular contributions to catalysis besides the K19−C22 ion pair.

BACKGROUND AND THEORY

The pK_a values were calculated according to the approach of Yang et al. (*23*) based on the thermodynamic cycle shown in Scheme 1 for protonation of a titratable group in solution (s*i*) and in the protein environment (p*i*). The particular program called "pK_a suite" was kindly provided by Dr. Yang

[1] Abbreviations: GSH, glutathione; NMR, nuclear magnetic resonance; NOE, nuclear overhauser effect; GRx, human glutaredoxin; SC-GRx, single cysteine glutaredoxin (C7S, C25S, C78S, and C82S); SC-GRx-SSG, single cysteine glutaredoxin in the mixed disulfide adduct with glutathione at Cys22; TM-GRx, triple mutant glutaredoxin (C7S, C78S, and C82S); TM-GRx-SSG, triple mutant glutaredoxin in the mixed disulfide adduct with glutathione at Cys22.

Scheme 1: Thermodynamic Cycles of a Titratable Group, *i*, Deprotonation in Solution (s) and in Protein (p) Environment

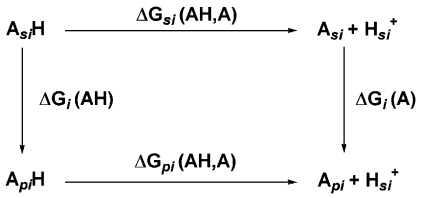

(see Acknowledgment). $A_{si}H$ and $A_{pi}H$ are the protonated states of the group in solution and in the protein, respectively; A_{si} and A_{pi} are the corresponding deprotonated states. H_{si}^+ represents the proton in solution. The procedure has been described in detail (*23*); therefore it is only summarized here.

The pK_a of the titratable residue *i* in the protein is given by

$$pK_{ai} = pK_{ai}^0 - \gamma(i)\frac{1}{2.303kT}[\Delta G_{pi}(AH,A) - \Delta G_{si}(AH,A)] =$$

$$pK_{ai}^0 - \gamma(i)\frac{1}{2.303kT}[\Delta G_i(A) - \Delta G_i(AH)] =$$

$$pK_{ai}^0 - \gamma(i)\frac{1}{2.303kT}\Delta\Delta G_i \quad (1)$$

where pK_{ai}^0 is the pK_a of the isolated amino acid in solution, ΔG(AH,A) is the free energy for acid dissociation, and ΔG(A) and ΔG(AH) are the changes in free energy for transfer of the deprotonated and protonated amino acid from solution to the protein environment as defined in Scheme 1. The pK_{ai}^0 values were 3.9 for Asp, 4.3 for Glu, 8.3 for Cys, 10.5 for Lys, 12.5 for Arg, and 6.5 for His. The factor $\gamma(i)$ equals -1 for acidic groups and $+1$ for basic groups. $\Delta\Delta G_i$, the difference in the free energy of ionization in solution relative to that in the protein, has three contributions (eqs a−c):

$$\Delta\Delta G_i = \Delta\Delta G_i^{rf} + \Delta\Delta G_i^{perm} + \Delta\Delta G_i^{ttr} \quad (a)$$

$\Delta\Delta G_i^{rf}$ refers to differences in the reaction field energy of desolvation, and $\Delta\Delta G_i^{perm}$ is the contribution from interactions with the permanent dipoles in the neutral protein. $\Delta\Delta G_i^{ttr}$ is the contribution from charge−charge interactions between residue *i* and the other titratable groups in the protein. It is pH dependent. The desolvation energy is

$$\Delta G^{rf} = \sum q_i \Delta\phi^{rf}/2 \quad (b)$$

where $\Delta\phi^{rf}$ is the difference in the reaction field potential at the charged atom in the isolated amino acid and in the protein. ΔG_i^{perm} is calculated from the potential, $\Delta\phi^{perm}$, arising from all the partial charges of the protein when the titratable groups are formally neutral but with partial charges assigned for each atom:

$$\Delta G_i^{perm} = \sum q_i \Delta\phi^{perm} \quad (c)$$

G_i^{perm} and G_i^{ttr} are equal to zero for the isolated amino acid.

A statistical mechanical treatment is needed to estimate charge−charge interactions among multiple titratable groups in calculating $\Delta\Delta G_i^{ttr}$ (*23*, *24*, *26*). For this purpose, it is convenient to determine an intermediate pK_a value, the intrinsic acid-dissociation constant pK_{ai}^{int}, which is defined as the pK_a of site *i* when all other titratable sites in the protein are neutral but carry partial charges. Thus pK_{ai}^{int} is given by eq 2

$$pK_{ai}^{int} = pK_{ai}^0 - \gamma(i)\frac{1}{2.303kT}[\Delta\Delta G_i^{rf} + \Delta\Delta G_i^{perm}] \quad (2)$$

and the pK_a of site *i* becomes $pK_{ai} = pK_{ai}^{int} - \Delta pK_{ai}^{ttr}$. The pH-dependent charge−charge interactions of all the titratable groups for estimating ΔpK_{ai}^{ttr} are obtained by calculating the titration curve for the system, and the pK_a at site *i* is the pH at which the group *i* is half-protonated. A hybrid statistical mechanical/Tanford−Roxby treatment provides efficient and accurate results for titration curves involving a large number of titratable groups, even in the case of strongly coupled interactions (*23*).

COMPUTATIONAL METHODS

Electrostatic Potential Calculations. DelPhi was used to solve the Poisson−Boltzmann equation by finite difference to estimate the electrostatic potential of the system (*27*, *28*). The difference in the reaction field potential $\Delta\phi_i^{rf}$ in the term ΔG_i^{rf} (eq 3) was obtained for the titratable residue in the protein with dielectric constant ϵ_{in} of 4 versus the isolated residue in solution with dielectric constant ϵ_{ex} of 80. The potential $\Delta\phi^{perm}$ for the free energy $\Delta\Delta G_i^{perm}$ (eq 4) is the potential at the site due to partial charges on residues in their neutral form. Partial charges from the CHARMM22 (*29*) or the cvff parameter sets (Accelrys, San Diego) were used in this study. The solvent-accessible surface was calculated for a 1.4 Å radius probe. The salt concentration was 0.2 M, and ions were excluded 2 Å from the surface. The grid number in each of three dimensions was set to 65 throughout the calculations. The focusing method was used to obtain more accurate boundary conditions. The residue of interest was first placed in the center of a box with 0.7 grid point/Å and the potential at each grid point calculated. A smaller grid box (better resolution) was used for subsequent runs with the potential at the edge of the grid box taken from the previous run. Four focusing runs were done with 0.7, 1, 2, and 4 grid points/Å.

Glutaredoxin Structures. The coordinates for 20 NMR structures for reduced human glutaredoxin (1jhb) (*22*) were obtained from the protein data bank (PDB) at Brookhaven National Laboratory. Cys22 is in the thiolate ionization state for the NMR structural analysis. The neutral and charged states of amino acids were modeled in each structure using the HBUILD facility of the CHARMM26 program to "build" hydrogen atoms in the lowest-energy position from the known heavy-atom coordinates. Hydrogen atoms were added to the appropriate heavy atom to generate charged His and neutral Asp and Glu side chains. The neutral Lys and Arg side chains were obtained by deleting one H^{ζ} proton and the H^{ϵ} proton, respectively.

Models for K19L and K19Q variants of GRx were generated by replacing Lys19 with the desired residue using the BIOPOLYMER module within the InsightII program (Accelrys, San Diego). The resulting structures were subjected to energy minimization using CHARMM26 with a 50.0 kcal/Å^2 harmonic restraint potential applied to the

atomic positions of residues within 8 Å of Cys22 while the coordinates of other residues were fixed. Residue 19 was allowed to move freely. The energy was minimized with the conjugate gradient algorithm until the rms gradient was less than 0.1 kcal/Å. After the minimization procedure, the system was subjected to simulated annealing molecular dynamics with a 5.0 kcal/Å^2 harmonic constraint applied to the main chain atoms of residues within 8 Å of Cys22, and atoms from other residues were fixed. Simulated annealing was carried out for 14 ps at 1000 K with slow cooling to 300 K. Finally, restrained energy minimization using the conjugate gradient algorithm was executed until the rms gradient was less than 0.05 kcal/Å. The Cys22 thiol was assumed to be ionized during the simulation. Five structures were generated from each NMR coordinate set. The structure with the lowest total energy was used for pK_a calculations.

K19Q-SC-GRx-SSG and *K19L*-SC-GRx-SSG were generated from the average NMR structure of SC-GRx-SSG (1b4q) (*14*). The NMR structure was first subjected to 200 steps of steepest-descent energy minimization using CHARMM26 without the electrostatic term, followed by a conjugate gradient minimization, including the electrostatic interactions with a 13 Å non-bond cutoff, until the rms gradient was less than 0.1. NMR distance and dihedral restraints were applied during the minimization to be consistent with the experimental NMR result. NOE interactions between protons on adjacent carbons, such as H$^{\alpha}$ and H$^{\beta}$, were not included in the calculations. The energy-minimized SC-GRx-SSG structure was used to model the glutathionyl mixed disulfide adducts of the mutant glutaredoxins. The Lys19 residue was replaced with either Gln or Leu residues, and the structures were subjected to energy minimization and simulated annealing following the same protocols as for GRx except that radial distances for applying harmonic restraints and fixed atoms were based on the glutathionyl moiety instead of Cys22. Five structures were generated, and the one with the lowest total energy was used for further analysis.

EMPIRICAL METHODS

Materials. Primers 5′-GTGTTCATCCAGCCCACCTGC-3′, 5′-GCAGGTGGGCTGGATGAACAC-3′, 5′-GTGTTCATCTTGCCCACCTGC-3′, and 5′-GCAGGTGGGCAAGATGAACAC-3′ for site-directed mutagenesis were purchased from Sigma-Genosys. The Quik-Change mutagenesis kit was from Stratagene. DH5α competent cells and the BL21(DE3) strain of *Escherichia coli* were from Invitrogen. Concert Miniprep kits were from Life Technologies. *Dpn*I and isopropyl-D-galactopyranoside (IPTG) were from Gibco. Sephadex and Q-Sepharose chromatography resins were from Pharmacia Biotech. Micro BCA protein assay was purchased from Pierce. Glutathione (GSH), glutathione reductase (GRase), 2-[*N*-morpholino]ethanesulfonic acid (MES), *N*-[2-hydroxyethyl]piperazine-*N*′-[2-hydroxy-propanesulfonic acid] (HEPPSO), iodoacetamide (IAM), dithiolthreitol (DTT), protamine sulfate, and chelating resin (Chelex) were from Sigma. Sodium phosphate, potassium phosphate, sodium acetate, sodium citrate, potassium chloride, and sodium chloride were from Fisher. Ammonium formate was from Aldrich. L-Cysteine glutathione disulfide (CSSG) was from Toronto Research Chemicals. NADPH was from Roche.

Design and Construction of Glutaredoxin Mutants. Site-directed mutagenesis was employed to mutate the lysine 19 residue of the single-cysteine glutaredoxin (C7S, C25S, C78S, C82S-GRx) to either a glutamine or leucine residue. The lysine 19 of triple mutant glutaredoxin (C7S, C78S, C82S-GRx) was mutated to a leucine residue by employing the same technique. Forward and reverse primers for each mutant were as follows: glutamine forward, 5′-GTG TTC ATC CAG CCC ACC TGC-3′; glutamine reverse, 5′-GCA GGT GGG CTG GAT GAA CAC-3′; leucine forward, 5′-GTG TTC ATC TTG CCC ACC TGC-3′; leucine reverse, 5′-GCA GGT GGG CAA GAT GAA CAC-3′. The templates, pET-24d-SC-GRx or pET-24d-TM-GRx, as well as forward and reverse primers, were added to a reaction mixture and allowed to go through 18 cycles of PCR. Following PCR, the parental strand was digested using *Dpn*I, leaving only the newly synthesized mutant DNA. The vectors containing the desired mutation were transformed into DH5α cells.

Standard Spectrophotometric Assay for Glutaredoxin Activity. The assay mix consisted of equal parts of (a) 0.66 mM NADPH/0.33 M sodium/potassium phosphate, pH 7.4, (b) 1.67 mM reduced glutathione (GSH), and (c) Chelex-treated deionized H_2O and 12 units of GSSG reductase; final concentrations in the reaction are 0.2 mM NADPH/0.1 M Na^+/K^+ phosphate, pH 7.4, 0.5 mM GSH, and 2 units of GSSG reductase. GRx was incubated in the assay mix for 5 min at 30 °C prior to the initiation of the reaction with 1 mM L-cysteine-glutathione-disulfide (CSSG); final concentration in the reaction mixture was 100 μM. The reaction was monitored for 5 min at 340 nm using a Molecular Devices ThermoMax microplate reader. One unit of GRx activity corresponds to 1 μmol of GSSG produced (NADPH oxidized) per minute under standard conditions. In some cases a modified assay was used which is the same as described above, except the final concentration of GSH was 0.25 mM and GSSG reductase content was 4 units/mL. The modified assay was used so that background reaction rates were lower than in the standard assay at high concentrations of CSSG.

Protein Purification. K19 mutant constructs were transformed into BL21(DE3) *E. coli* competent cells. Cells were cultured until reaching an A_{600nm} of 1.0 and then induced with 1 mM IPTG to overexpress GRx. After 5−6 h at 37 °C, the cells were centrifuged at 6000*g* for 15 min at 4 °C. The pellet was resuspended in 10 mM K^+ phosphate, pH 7.4, and 1 mM DTT. A French press was used to lyse the cells at a pressure less than or equal to 5000 psi. The lysate was centrifuged at 48000*g* for 20 min at 4 °C to remove cellular debris. The supernatant was treated with 25 mg/mL protamine sulfate according to the A_{260nm} reading to remove nucleic acids, as described previously (*14*). The precipitated nucleic acids were removed by centrifugation at 48000*g* for 20 min at 4 °C. The supernatant was heat treated in a 60 °C water bath to remove heat sensitive proteins. Precipitated proteins were removed by centrifugation at 48000*g* for 20 min at 4 °C. The treated protein solution was poured over a Sephadex G-75 size exclusion chromatography column preequilibrated at 4 °C with running buffer, 10 mM ammonium formate, pH 5.8. The elution flow rate was 0.5 mL/min. Fractions were collected and tested for GRx activity and total protein content, using the standard GRx assay and

Micro BCA assay, respectively. Those fractions with the highest and nearly constant specific activity were pooled. A final purification was accomplished by passing the pooled fractions over a Q-Sepharose Fast Flow column to remove any contaminating nucleic acids. The pure sample was concentrated and confirmed as a single band on SDS−PAGE and/or HPLC as described previously (*14*). It was then adjusted to a 20% glycerol stock and stored at −80 °C.

Mass Spectral Analysis. Mass spectral analysis was used to determine if the K19 mutants remained specific for the glutathionylated disulfide substrate. SC-GRx (39 μM) was incubated with 245 μM CSSG, 28 μM K19Q SC-GRx was incubated with 245 μM CSSG, and 61 μM K19L SC-GRx was incubated with 800 μM CSSG. The samples were incubated for 20 min at 30 °C. The reaction vial was then placed at 4 °C pending mass spectral analysis. Mass spectral analysis was performed on a Finnigan LCQ electrospray mass spectrometer operated by Paul Minkler (VA Medical Center, Cleveland), as described previously (*14*). Exclusive adduction of the glutathionyl moiety (mass addition of +306 Da) was indicative of specificity (see Results).

Kinetic Characterization. The K_m and V_{max} values for SC-GRx and the two mutants with the CSSG substrate were determined using the standard or modified assay for GRx activity. Instead of initiating with 1 mM CSSG, the reactions were initiated with CSSG concentrations ranging from 0.05 mM to 10 mM. The final concentrations of CSSG in the assay ranged from 5 μM to 1 mM. The concentrations of SC-GRx, K19Q SC-GRx, and K19L SC-GRx in the assay were 9 nM, 108 nM, and 154 nM, respectively, reflecting their relative specific activities. The concentrations of TM-GRx, K19Q TM-GRx, and K19L TM-GRx in the assay were 17 nM, 52 nM, and 52 nM, respectively, reflecting their relative specific activities.

pH Dependence of Iodoacetamide Inactivation of GRx. To determine the pK_a of the active site cysteine, the enzyme was incubated with iodoacetamide, a thiol selective alkylating agent, at different pH values and then assayed for activity, analogous to our previous studies (*20*). The desired concentration of enzyme (WT-GRx, 0.66 μM; TM-GRx, 0.66 μM; SC-GRx, 1 μM; K19Q SC-GRx, 14 μM; K19L SC-GRx, 16 μM; K19Q TM-GRx, 7 μM; K19L TM-GRx, 3 μM) was incubated with 300 μM iodoacetatmide (IAM) and pH buffer for 3 min at room temperature. A 100-fold dilution of the reaction mixture into an ice-cold assay mix quenched the iodoacetamide reaction. Activity of the enzyme was determined using the standard assay for GRx activity. The percent activity remaining after treatment with iodoacetamide was determined by comparing the GRx activity of samples incubated in the presence and absence of iodoacetamide at the indicated pH values. Buffers used were as follows: Na citrate, pH 2.0, 3.0, and 3.5; Na acetate, pH 3.5, 4.0, 4.5, and 5.0; MES, 5.0, 5.5, 6.0, and 7.0; and HEPPSO, pH 7.0, 8.0, and 9.0. All buffers were 10 mM in concentration, and ionic strength was adjusted to 0.5 M in all cases by addition of the appropriate amount of NaCl or KCl

RESULTS AND DISCUSSION

Computational Studies. pK_a of Cys22 Side Chain. The conformational variation inherent to NMR structures was exploited to try to understand the chemical origin of the very low pK_a value for Cys22. The calculated pK_a value for Cys22 in the 20 NMR structures of reduced human GRx varied between 4.1 and 10.5 when calculated with the CHARMM partial charge set, and between 4.1 and 11.5 with the cvff partial charge set (Figure 2A). This large range in pK_a values is due to the conformational differences among the NMR structures, while the results are relatively insensitive to the choice for partial charges. Specific contributions illustrated with the cvff charge set (Figure 2B) show that interactions of Cys22 with the partial charges and ionizable groups of the protein are favorable while desolvation is not favored in the protein, as expected. We note that the $\Delta\Delta G^{perm}$ and $\Delta\Delta G^{rf}$ terms are strongly inversely correlated, corresponding to the opposing energetic effects from intramolecular protein Coulombic interactions and desolvation, as recognized previously (*30*). The structural basis for the range of pK_a values was examined, and a strong interaction with Lys19 and a smaller desolvation penalty were found to be the major factors for reducing the pK_a value of Cys22. The NMR structures distribute into four groups with respect to their calculated pK_a values. In structures 1−4 (Figure 3A), the side chains of Cys22 and Lys19 are in close contact; the distance between Lys19 N^{ϵ} and Cys22 S^{γ} is less than 2.5 Å (Figure 2C). The average contribution to the charge−charge free energy of Cys22 S^{γ} from the Lys19 residue for these four structures is −6.5 kcal/mol, corresponding to a 4.7 unit decrease in the Cys22 pK_a, i.e., the proximity of Lys 19 accounts for a decrease in pK_a of Cys22 from 8.3 to 3.6. An increase in the salt concentration from 0.2 M to 2 M did not significantly affect the calculated charge−charge interaction energy (−6.1 kcal/mol) with the Lys19 charged side chain. This result is consistent with the experimental observation that changing the ionic strength from 0.05 to 2 M does not affect the apparent pK_a of the Cys22 thiolate (*20*). Upon close examination of these structures one finds that the methylene groups of the Lys19 side chain interact with several

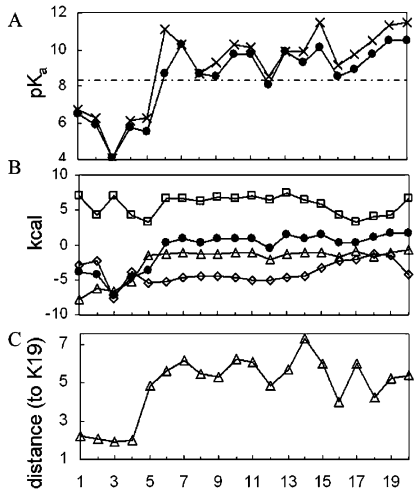

FIGURE 2: Electrostatic analysis of the Cys22 thiolate. The NMR structures are numbered so that those with lower calculated pK_a values are designated 1−5, and structures with higher calculated pK_a values are 6−20. The horizontal dotted line is at 8.3, the pK_a of cysteine thiol in solution. Plot A: Calculated Cys22 pK_a values for the 20 PDB NMR structures using the CHARMM22 partial charge set (●) or cvff partial charge set (×). Plot B: Free energy contributions from desolvation energies $\Delta\Delta G^{rf}$ (□), permanent dipole $\Delta\Delta G^{perm}$ (◇), charge−charge interactions (△), and the sum of the three terms (●). Plot C: Distance (in Å) between Lys19 N^{ϵ} and Cys22 sulfur. The *x*-axis is structure number.

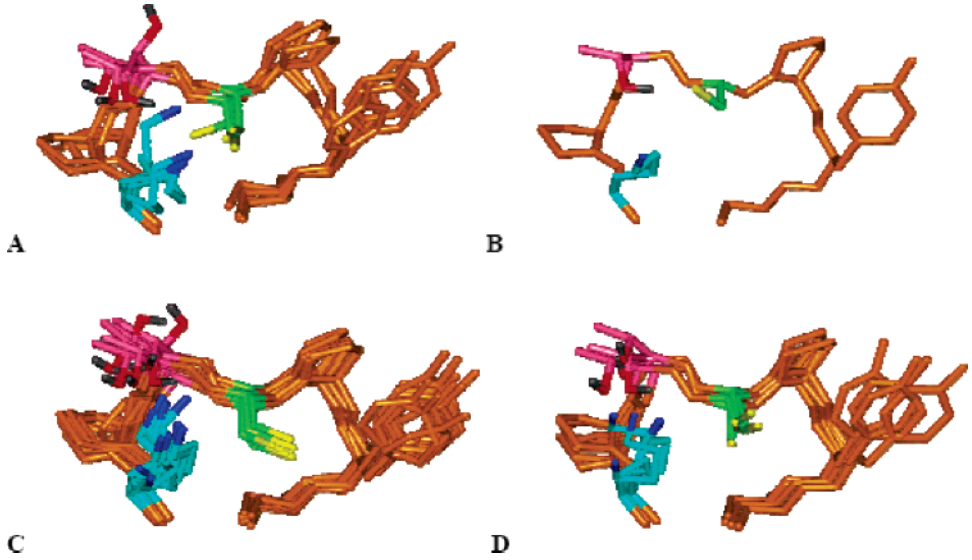

FIGURE 3: Four groups of structures classified according to calculated pK_a values: Cys22 is shown in yellow, Thr21 is shown in red, and Lys19 is shown in blue. (A) These structures (1 to 4) gave calculated pK_a values below 8.5. (B) This structure (5) gave a pK_a value of 5.5 *but did not form an ion pair with Lys19*. (C) Overlap of structures (6 to 16) with conformations that gave calculated pK_a values above 8.5 because of high $\Delta\Delta G^{rf}$ values. (D) Overlap of structures (17 to 20) with conformations that gave calculated pK_a values above 8.5 because of high $\Delta\Delta G^{perm}$ values.

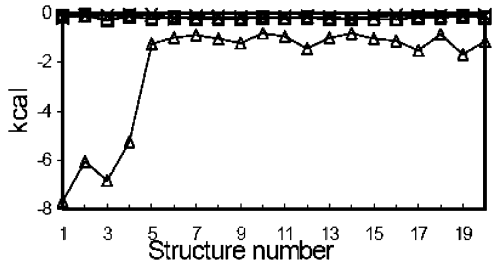

FIGURE 4: Calculated potentials from Lys19, Arg26, and Arg27 on the Cys22 S^{γ} (Lys19, △; Arg26, □; Arg27, ×). For these calculations, the salt concentration was set to 0.2 M.

hydrophobic residues, such as the Thr48 methyl group, Ile47, and Val69. These interactions can sequester the ammonium charged group in a relatively solvent-inaccessible space. In contrast, other nearby basic residues, Arg26 and Arg27, have well-solvated side chains and the interactions would be less effective compared to Lys19 in stabilizing the C22 thiolate. As shown in Figure 4, the most favorable potential at the position of the Cys22 thiolate arising from Arg26 and Arg27 among 20 NMR structures is −0.28 kcal/mol and −0.22 kcal/mol, respectively. Furthermore, these interactions depend strongly on ionic strength; the values decrease by a factor of 2 when the salt concentration increases to 2 M. Wells et al. proposed that Arg26 is responsible for the low pK_a of Cys22 according to iodoacetamide-inactivation studies of the R26V variant and the R26V, K27Q double variant of pig liver glutaredoxin (*17*). The iodoacetamide reactivities of both variants were very low and pH independent over the range pH 2.5 to pH 8.5 compared to the wild-type enzyme, which displayed a typical titration profile over the pH range 2.5 to 4.5. This result is anomalous, suggesting that the apparent pK_a of Cys22 in the mutants would be greater than 8.5. Since R26 and K27 appear to be well solvated normally, the loss of IAA reactivity may be better interpreted as a lack of accessibility of the Cys22-thiol in the mutant enzymes to IAA, rather than to simple removal of the positive side chains of Arg26 and/or Lys27.

In the second group (Figure 3B), the structure (5) is predicted to have a low pK_a value for Cys22 equal to 5.5, but the contact between Cys22 and Lys19 is not close. In this case a more favorable $\Delta\Delta G^{perm}$ reflects stabilization of the Cys22 thiolate by hydrogen bonding interactions involving Cys22 with the hydroxyl side chain of Thr21 and the backbone NH, as well as numerous other weaker polar interactions. The hydrogen bond interaction between Cys22 and Thr21 is also found in one structure of the group shown in Figure 3A. This structure (3) has a predicted pK_a equal to 4.1 which is about 2 units lower than the values for the other three structures. In addition to $\Delta\Delta G^{perm}$, the second group (structure 5) has a reduced magnitude of $\Delta\Delta G^{rf}$. This diminution in the desolvation penalty for the charged thiolate within the protein is a property of the overall conformation for this structure. A relatively favorable $\Delta\Delta G^{perm}$ due to Thr21 and other polar interactions, combined with a reduced magnitude $\Delta\Delta G^{rf}$ (Figure 2), leads to the reduced pK_a for this structure being a result of a more general feature of this protein conformation, rather than a single primary electrostatic interaction. Nonetheless, both ion-pair interactions with Lys19 and hydrogen bonding with Thr21 are candidates for serving to lower the pK_a of Cys22. Since the estimated stabilization from Lys19 is observed in four structures to be considerably stronger than that from Thr21, variants of Lys19 were studied in silico and then tested empirically (see below).

Structures 6 to 16 are predicted to have pK_a values greater than 8.5 and have a buried Cys22 side chain but no stabilizing interaction with Lys19 (Figure 3C**)**. As such, formation of a charged thiolate would be highly unfavorable given this conformation. Here, the unfavorable $\Delta\Delta G^{rf}$ values are offset by favorable $\Delta\Delta G^{perm}$, but are not further compensated by significantly low $\Delta\Delta G^{ttr}$ values. The overall result is high pK_a values (Figure 2A,B).

In the final group of structures (17 to 20) (Figure 3D), high pK_a values are predicted even though the Cys22 side chain is better solvated and shows more favorable $\Delta\Delta G^{rf}$ values (Figure 2B). In keeping with the inverse correlation

in $\Delta\Delta G^{perm}$ and $\Delta\Delta G^{rf}$ noted above, an increase in $\Delta\Delta G^{perm}$ due to fewer interactions with partial charges accompanies the decrease in $\Delta\Delta G^{rf}$. As a result, the pK_a of Cys22 is relatively high.

As seen in the present study, pK_a calculations are sensitive to local conformation. The pK_a values calculated from NMR structures in which Cys22 thiolate interacts with Lys19 and/or Thr21 are lower and more consistent with the reported experimental value of 3.5 (*6*, *20*). The pK_a values calculated for structures in which Cys22 interacts weakly with Lys19 are substantially greater than the experimental value. Based on the conformations calculated to have low pK_a values, we would conclude that a strong Cys22−Lys19 interaction is the basis for stabilization of the thiolate ion and the altered pK_a of Cys22 in GRx. Further, since the structures with a short Cys22−Lys19 distance yield good agreement between the predicted pK_a and previous experimental results for the wild type enzyme, these structures are considered more likely representative of reduced glutaredoxin in solution, while the other NMR structures with predicted pK_a values near neutral or higher cannot be heavily populated. Therefore the NMR structure which gave the most reasonable pK_a value, i.e., consistent with previous empirical data, was chosen as the starting structure for constructing K19Q and K19L mutants.

Similar calculations have been reported using NMR structures for *E. coli* thioredoxin (*25*) whose active-site thiol group of Cys32 has a pK_a value near neutral. Interaction with the thiol of Cys35 (analogous to Cys25 in glutaredoxin) was found to modulate the pK_a of Cys32 (analogous to Cys22 in glutaredoxin). Although 13 out of 20 NMR structures for glutaredoxin have a hydrogen bond interaction between Cys 25 γH and the Cys22-thiolate (*22*), this interaction does not significantly lower the pK_a of Cys22 according to our calculations. However, mutation of Cys25 (C25S) does change the impact of Lys19 mutations on the pK_a of Cys22. No positive side chain is found in proximity to Cys32 for thioredoxin, unlike the case for glutaredoxin Cys22. This distinction for the stabilization of the catalytic cysteine thiolate between Lys19 (glutaredoxin) and Cys35 (thioredoxin) suggests a basis for the different catalytic mechanism of the two enzymes (*6*, *14*, *16*, *18*). The moderately lowered pK_a of the C35-thiolate on thioredoxin serves as a better nucleophile to initiate the first step of attack on the disulfide substrate. On the other hand, the very low pK_a of the C22-thiolate on glutaredoxin serves as a better leaving group in the second step involving GSH attack on the GRx-SSG intermediate to turn over the enzyme (*18*).

$$\mathbf{R}_{nuc}S^- + S\text{-}S\mathbf{R}_{lg} \rightarrow \underset{\mathbf{R}_c}{\mathbf{R}_{nuc}S^-\ldots S\ldots S\mathbf{R}_{lg}} \rightarrow \underset{\mathbf{R}_c}{\mathbf{R}_{nuc}S\text{-}S} + {}^-S\mathbf{R}_{lg}$$

For a typical thiol−disulfide exchange reaction where a thiolate anion (R_{nuc}) attacks one of the two sulfurs of the disulfide bond, the central sulfur (S-R_c) will be the one with higher pK_a. The lower the pK_a of the leaving sulfur (SR_{lg}), the faster the rate, according to the Brønsted linear free energy relationship (*31*):

$$\log k = c + \beta_{nuc}\, pK_{a(nuc)} + \beta_c\, pK_{a(c)} + \beta_{lg}\, pK_{a(lg)}$$

For reactions occurring at physiological pH (pH = 7.4), lowering the pK_a of the nucleophilic thiol increases the reaction rate simply by increasing the concentration of thiolate species. When the pK_a of the thiol is 6.0, >90% of the nucleophile is in the thiolate form at pH 7.4. Further decrease in pK_a would not increase the thiolate concentration substantially, and actually detracts from the rate of the reaction as nucleophile (*31*). Nevertheless, the initial reaction of the enzyme with the disulfide substrate occurs rapidly, and the turnover of the enzyme−SSG intermediate is rate limiting. Thus, the active cysteine of glutaredoxin (Cys22, pK_a 3.5) provides the catalytic advantage by serving as the leaving group (*18*). Cys32 of thioredoxin (pK_a = 6.7), on the other hand, is more likely to enhance only the rate of nucleophilic attack and have little effect as leaving group.

Prediction of Glutathionyl Specificity of the K19Q-SC-GRx-SSG and K19L-SC-GRx-SSG Mutants from Steric Considerations of the Glutathionyl Moiety with Adjacent Protein Residues. As a first approximation to evaluate the effect of the K19Q and K19L mutations on the specificity for glutathione, the steric fit at residue 19 was characterized from nonbonded interactions. Electrostatic and van der Waals energies were calculated (using structures generated as described under Computational Methods) between the adducted glutathionyl moiety and protein residues within 8 Å of this moiety. The nonbonded energies for *K19Q*-SC-GRx-SSG and *K19L*-SC-GRx-SSG were −184 and −185 kcal/mol, respectively, compared to −192 kcal/mol for *WT*-SC-GRx-SSG. The difference is less than a 5% change, despite the loss of ionic interactions with a Lys residue, and suggests that the variant proteins could stabilize the glutathionyl moiety similarly to wild type. The Arg67 side chain moves closer to the peptide carboxyl group of Gly 3′ during the molecular dynamics of modeling to help stabilize both variant forms. Thus it is predicted that recognition of glutathione would not change substantially for either of the mutants at the first step of catalysis where the GRx-SSG intermediate is formed, and that glutathionyl specificity should be retained. This prediction was borne out by the empirical data (see below).

pK_a *Values for the Cys22-Thiol Moiety of the K19Q and K19L Mutants of Glutaredoxin.* K19Q and K19L variants of glutaredoxin were modeled as described in Computational Methods. The pK_a values estimated by the same procedure used for the wild-type enzyme are 7.3 and 8.3, respectively. According to the calculations, only small perturbations on the pK_a result from the protein environment, consistent with Lys19 being the major source of stabilization of the Cys22 thiolate. Structures of the two variants are shown in Figure 5 superimposed on the wild-type protein structure corresponding to the lowest calculated pK_a value (structure 3, pK_a = 4.1). Structural perturbations due to the mutations are localized to side-chain conformations. The primary basis for the difference in pK_a values between the two variants and the wild-type enzyme is the ΔG^{ttr} term (charge−charge interactions) (Figure 6). The basis for this difference is clear in Figure 5; the charge−charge interaction of the wild type between Lys19 and Cys22 thiolate is only partially compensated by the hydrogen bonding interaction with Gln19 in one variant and eliminated altogether by the Leu19 substitution. These conformational factors are reflected in the lower Cys22 $\Delta\Delta G^{perm}$ and associated pK_a value of the K19Q variant. These calculations show some qualitative

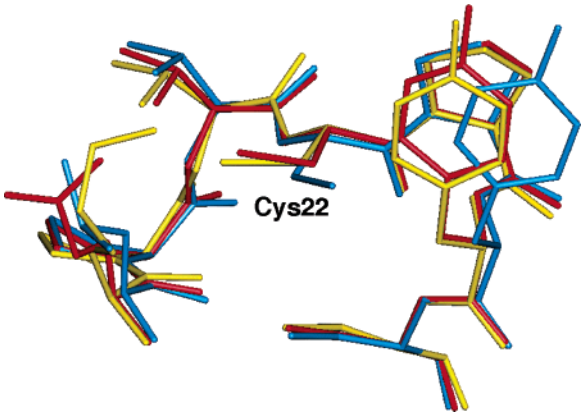

FIGURE 5: Superimposition of the active site of glutaredoxin (yellow), K19Q mutant (red), and K19L mutant (blue).

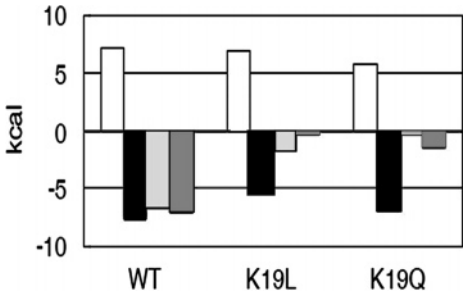

FIGURE 6: Comparison of free energy contributions from desolvation, permanent dipole, and charge−charge interactions for wild-type glutaredoxin and the K19L and K19Q mutants. The patterns of bars are as follows: no fill for $\Delta\Delta G^{rf}$, black for $\Delta\Delta G^{perm}$, light gray for the charge−charge interactions $\Delta\Delta G^{ttr}$, and dark gray for the total free energy.

agreement but do not correspond quantitatively to what is found empirically for the K19 variants (see below).

Empirical Studies of Glutaredoxin K19 Mutants. The NMR study that served as a basis for modeling the K19 mutants was performed using the single-cysteine glutaredoxin (SC-GRx; C7S, C25S, C78S, C82S) (*14*). SC-GRx lacks all cysteines except the catalytically active Cys22. This form of the enzyme obviates the formation of any nonspecific intra- or intermolecular disulfide bonds, which might complicate the kinetics. It was previously shown to retain specificity for glutathione-containing disulfide substrates (*14*). Therefore, it was chosen as one of the forms of the GRx protein in which to test the K19 mutations. SC-GRx differs from WT-GRx in that it has a V_{max} and K_m 2-fold higher than the wild-type enzyme, which is consistent with its inability to form an intramolecular C22−C25 disulfide, which detracts from catalysis (*14*) (see Figure 1). A second cysteinyl mutant of glutaredoxin that we characterized previously was also used to test the K19 mutations. This enzyme, triple mutant glutaredoxin (TM-GRx; C7S, C78S, C82S), retains both Cys22 and Cys25, which reside at the active site. TM-GRx has kinetics indistinguishable from those of WT-GRx, and it was used to evaluate how the K19 mutations would affect WT-GRx properties without potential complications from the peripheral cysteines (*14*).

Studies of Substrate Specificity. Mass spectrometry was utilized, as described previously (*14*), to assess whether mutation of the lysine 19 residue of GRx would affect the specificity of the enzyme for glutathionylated substrates. Computational modeling predicted that the selected isosteric mutations of K19 would not interfere with the substrate specificity of the enzyme. The K19 SC-GRx mutants, as well as SC-GRx, were incubated with a 10-fold excess of L-cysteine-glutathione disulfide (CSSG), in the absence of glutathione, such that the enzyme was trapped in the intermediate disulfide form. For SC-GRx, like WT-GRx, it is known that the intermediate form of the enzyme is GRx-SSG (*13*, *14*). This form can be detected through mass spectral analysis by exclusive adduction of the 306 Da moiety to the enzyme (*14*), distinguishing glutathionyl-enzyme disulfide formation from cysteinyl adduction derived from the other half of the CSSG. For each K19 SC-GRx mutant, as for SC-GRx, only one peak was detected, showing a 306 Da shift relative to the unreacted enzyme. These results document exclusive adduction of the glutathionyl moiety and confirm retention of enzyme specificity in the K19 mutants. Had either mutant lost specificity, an equal mixture of the glutathione-adducted enzyme and cysteinyl-adducted enzyme would have been observed. Such nondiscrimination was documented when the analogous single-cysteine mutant form of thioredoxin was reacted with cysteine-glutathione disulfide (CSSG) (*14*).

Kinetic Characterization of K19 GRx Mutants. The relationship between the pK_a of the leaving group and the overall catalytic rate of the enzymatic reaction for thiol disulfide exchange reactions can be explained using the Brønsted linear free energy relationship ($\log k = c + \beta_{nuc}\, pK_{a(nuc)} + \beta_c\, pK_{a(c)} + \beta_{lg}\, pK_{a(lg)}$), as decribed above. Accordingly, for a given homologous set of thiol disulfide exchange reactions, each one-unit decrease in the pK_a of the leaving group corresponds to a 4-fold increase in the second-order rate constant; i.e., the relative rates are given by $\Delta k = 4^{(\Delta pK_a)}$ (*31*, *32*). Srinivasan et al. showed this to fit for GRx-mediated deglutathionylation of BSA-SSG (*18*). This concept is illustrated by the modeling predictions described above. Mutation of the K19 residue was predicted to increase the Cys22 pK_a and thereby decrease enzyme activity. Accordingly, The K19Q and K19L mutants were predicted to retain only 0.5% and 0.1% of wild-type activity, respectively.

Kinetic characterization of both sets of K19L and K19Q mutants relative to SC-GRx and TM-GRx was carried out using the modified assay of GRx activity (see Empirical Methods). All of the K19 mutants demonstrated a decrease in the apparent V_{max} relative to the corresponding parental enzymes (see Figures 7 and 8; Tables 1 and 2). K19L-SC-GRx and K19Q-SC-GRx exhibited 33% and 20% of SC-GRx activity. K19L-TM-GRx and K19Q-TM-GRx both displayed approximately 21% of TM-GRx activity. Based on the Brønsted linear free energy relationship as previously applied to the WT-GRx enzyme (*18*), V_{max} is dependent on the pK_a of the C22-thiolate as leaving group. Accordingly, decreases in V_{max} for the mutants would be attributed to increases in the pK_a of the C22-thiolate, as predicted by the computational analysis (above).

An important alternative explanation for the decrease in apparent V_{max} is focused on the nucleophilicity of the second substrate, GSH, which is responsible for turning over the enzyme intermediate. Srinivasan et al. showed that GSH has an enhanced nucleophilicity with respect to other thiol compounds in turning over GRx-SSG (*18*). Thus, mutation of the lysine 19 may interfere with the interaction between the glutathionylated enzyme intermediate and GSH, which

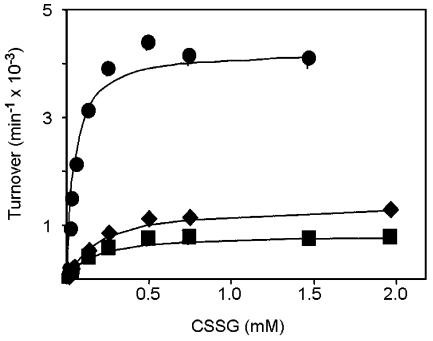

FIGURE 7: Kinetic parameters for SC-GRx (●), K19Q SC-GRx (■), and K19L SC-GRx (◆). A modified assay for glutaredoxin activity was used to determine V_{max} and K_m. The concentrations of L-cysteine-glutathione disulfide (CSSG), the prototype substrate, were varied as indicated, while the concentration of glutathione (GSH), the second substrate, was held at a fixed concentration of 0.25 mM. The concentration of the coupling enzyme, glutathione reductase (GRase), was 4 units/mL. The concentrations of SC-GRx, K19Q SC-GRx, and K19L SC-GRx in the assay were 9 nM, 108 nM, and 154 nM, respectively, reflecting their relative specific activities. Where error bars are not evident, they are within the limits of the symbol.

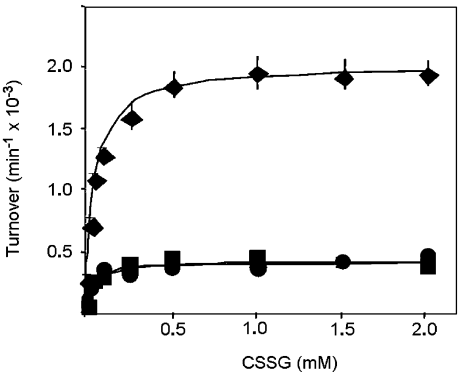

FIGURE 8: Kinetic parameters for TM-GRx (◆), K19Q TM-GRx (■), and K19L TM-GRx (●). A modified assay for glutaredoxin activity was used to determine V_{max} and K_m. The concentrations of L-cysteine-glutathione disulfide (CSSG), the prototype substrate, were varied as indicated, while the concentration of glutathione (GSH), the second substrate, was held at a fixed concentration of 0.25 mM. The concentration of the coupling enzyme, glutathione reductase (GRase), was 4 units/mL. The concentrations of TM-GRx and K19L TM-GRx in the assay were 17 nM and 52 nM, respectively, reflecting their relative specific activities. Where error bars are not evident, they are within the limits of the symbol.

Table 1: Kinetic Properties for SC-GRx, K19L SC-GRx, and K19Q SC-GRx

GRx form	V_{max} (min^{-1})	K_m[a] (μM)	V_{max}/K_m ($min^{-1}\,\mu M^{-1}$)	Cys22 pK_a (pH)
SC (WT)	4200	92	46	4.2
K19L	1400	480	3	4.6
K19Q	820	290	3	5.0

[a] CSSG at 0.25 mM GSH. See Empirical Methods and captions to Figures 7 and 10 for experimental details.

may alter the efficiency of GSH as the second substrate and decrease the V_{max} of the reaction. This possibility is suggested by analogy to the glutathione-S-transferase mechanism, where GSH binding to glutathione-S-transferase A1-1 requires the α-carboxylate of glutathione to be present for catalysis to occur (*33*). Allardyce et al. reported that glutathione binding to glutathione-S-transferase induces a conformational change leading to a change in apparent affinity for the second substrate in the reaction (*34*). A similar scenario can be envisioned in the case of GRx. Interaction of GSH with the GRx-SSG intermediate may induce a conformational change leading to destabilization of the disulfide bond of the intermediate, thus enhancing turnover of the enzyme. Pertinent to this consideration, the average NMR structure of SC-GRx-SSG shows the K19 ammonium ion in association with the carboxylate of the glycine moiety of glutathione (*14*); therefore it is reasonable that substitutions at the K19 position may alter the efficiency of formation of the GRx-SSG intermediate and/or the orientation of the disulfide bound glutathionyl moiety.

Table 2: Kinetic Properties for TM-GRx, K19L TM-GRx, and K19Q TM-GRx

GRx form	V_{max} (min^{-1})	K_m[a] (μM)	V_{max}/K_m ($min^{-1}\,\mu M^{-1}$)	Cys22 pK_a (pH)
TM (WT)	2000	40	50	3.6
K19L	410	35	12	3.7
K19Q	420	48	9	3.7

[a] CSSG at 0.25 mM GSH. See Empirical Methods and captions to Figures 8 and 10 for experimental details.

pH Dependence of Iodoacetamide Inactivation of Glutaredoxin Mutants: C22 pK_a Values. Molecular modeling predicted an increase in pK_a of the active site cysteine from 3.5 to 7.3 for the K19Q mutant and from 3.5 to 8.3 for the K19L mutant. The pH dependence of inactivation of the respective mutant glutaredoxin enzymes by iodoacetamide was used to determine the pK_a values of their active site cysteines (see Empirical Methods). The pK_a of SC-GRx was determined to be 4.2 ± 0.09, a value which agrees with previous data (*35*) (see Figure 9). The pK_a values for the K19L-SC-GRx and the K19Q-SC-GRx mutants were determined to be 4.6 ± 0.05 and 5.0 ± 0.11, respectively (see Figure 9). Consistent with the V_{max} values for the K19-SC-GRx mutants, the pK_a values relative to the parental enzyme were increased; however, the magnitude of the changes was considerably less than predicted by the modeling. The diminution in activity is qualitatively consistent with the theoretical calculations (above). However, the discrepancy between the predictions and the experimental outcome defeats the hypothesis that the K19−C22 ion pair deduced from the NMR structure of WT-GRx (*22*) is the sole basis for the low pK_a of the C22-thiolate.

A very different relationship was found between predicted and experimentally observed pK_a values for the K19 mutants in the TM-GRx background. The pK_a values for TM-GRx, K19L-TM-GRx, and K19Q-TM-GRx were determined to be 3.6 ± 0.06, 3.7 ± 0.09 and 3.7 ± 0.08 (see Figure 10). Thus, in the TM-GRx background the decreases in V_{max} values for the K19 mutants do *not* correspond to increases in pK_a; i.e., essentially no changes in pK_a were observed. One explanation for disengagement between changes in activity and changes in pK_a for the K19 mutants of TM-GRx might come from a change in the relative contribution of the side reaction in which the GRx-SSG intermediate spontaneously forms an intramolecular disulfide (as depicted in Figure 1). This side reaction diminishes the steady-state level of GRx-SSG and requires more GSH (higher apparent K_m for GSH) to drive the intramolecular disulfide back into the catalytic cycle. This relationship was demonstrated previously by the distinction between the kinetics of WT-GRX and TM-GRx relative to

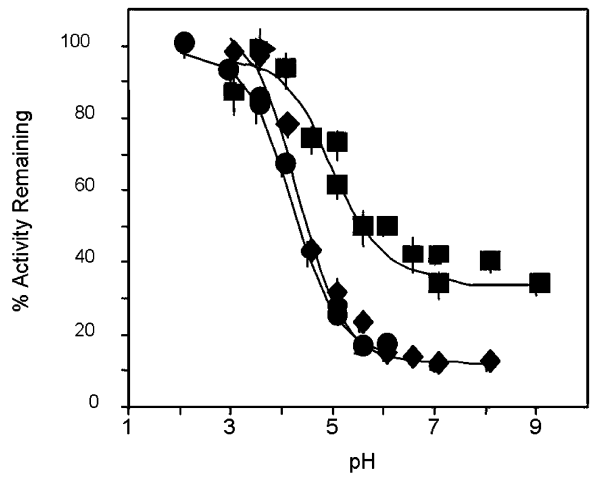

FIGURE 9: Cys22 pK_a determination for SC-GRx and K19 SC-GRx mutants. The pH dependence of iodoacetamide inactivation of SC-GRx (●), K19Q SC-GRx (■), and K19L SC-GRx (◆) was used to determine the pK_a of Cys22. To determine the pK_a of the active site cysteine, the enzymes were incubated with iodoacetamide (IAM), a thiol selective alkylating agent. The desired concentration of enzyme (SC-GRx, 1 μM; K19Q SC-GRx, 14 μM; and K19L SC-GRx, 16 μM) was incubated with 300 μM IAM for 3 min at room temperature and then assayed using the standard assay for glutaredoxin activity after a 100-fold dilution into the assay mix. Buffers used were as follows: Na citrate, pH 2.0, 3.0, and 3.5; Na acetate, pH 3.5, 4.0, 4.5, and 5.0; MES, 5.0, 5.5, 6.0, and 7.0; HEPPSO, pH 7.0, 8.0, and 9.0. All buffers were 10 mM in concentration, and ionic strength was adjusted to 0.5 M in all cases by addition of the appropriate amount of NaCl or KCl.

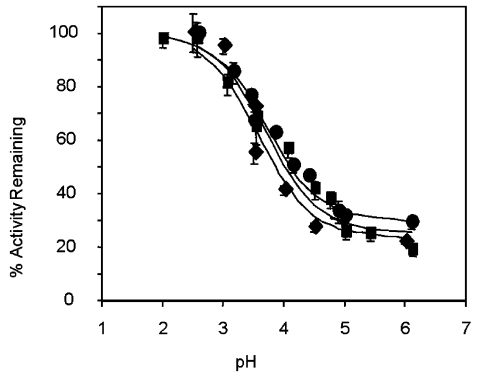

FIGURE 10: Cys22 pK_a determination for TM-GRx and its K19Q and K19L mutants. The pH dependence of iodoacetamide inactivation of TM-GRx (◆), K19Q TM-GRx (■), and K19L SCGRx (●) was used to determine the pK_a of Cys22. To determine the pK_a of the active site cysteine, the enzymes were incubated with iodoacetamide (IAM), a thiol selective alkylating agent, at different pH values. The desired concentration of enzyme (TM-GRx, 0.65 μM; K19Q TM-GRx, 7 μM; and K19L TM-GRx, 3 μM) was incubated with 300 μM IAM and then assayed using the standard assay for glutaredoxin activity after a 100-fold dilution into the assay mix. Buffers used were as follows: Na citrate, pH 2.0, 3.0, and 3.5; Na acetate, pH 3.5, 4.0, 4.5, and 5.0; MES, 5.0, 5.5 and 6.0. All buffers were 10 mM in concentration, and ionic strength was adjusted to 0.5 M in all cases by addition of the appropriate amount of NaCl or KCl.

SC-GRx which cannot form the intramolecular disulfide (*14*). Thus, the overall reaction rate depends on the concentration of the GRx-SSG intermediate, and any change in its steady state concentration correspondingly would affect the overall reaction rate. However, this steady state appears to be affected by different mechanisms in the SC-GRx form of the enzyme compared to TM-GRx. With SC-GRx, V_{max}, C22 thiol pK_a, and K_m for the first substrate (cysteinyl-glutathionyl-disulfide, CSSG) are all altered by mutation of K19 (Figure 7 and Table 1). This situation focuses the interpretation on changes in the first step of the catalytic reaction, i.e., formation of the GRx-SSG intermediate. As described above, an ion-pair interaction involving the K19 ammonium ion and the carboxylate of the disulfide-adducted glutathionyl moiety of the SC-GRx-SSG intermediate may be an important contributing factor to the efficiency of formation of the intermediate. Accordingly the K_m for the CSSG substrate would be increased by substituting uncharged amino acids for K19.

On the other hand, in the TM-GRx background mutation of K19 decreases V_{max} but does not alter the C22-thiol pK_a or the K_m for the first substrate CSSG (Figure 8 and Table 2). This remarkably focused effect implicates a selective change in the second step of the reaction scheme (Figure 1), in particular a change in the special effectiveness (nucleophilicity) of GSH as the second substrate relative to other thiol compounds. In other words, no change in K_m for CSSG focuses attention on a chemistry effect in step 2, likely involving the relative orientation of the disulfide bound glutathionyl moiety and the incoming GSH as second substrate, or stabilization of the deprotonated form of GSH. Either of these possibilities could involve ion pairing with the K19 ammonium moiety and be disrupted by replacement of K19. Hence control of local conformation, involving the C25 residue, may distinguish the kinetic effects of mutating the K19 residue.

The mutations of K19 were originally performed using the SC-GRx form of the enzyme under the assumption that the C25S mutation would have little effect on the pK_a of the active site cysteine (C22). However, the C25S change does have a significant effect on the C22 pK_a, raising it from 3.6 for WT-GRx to 4.2 for SC-GRx. This indicates that Cys25 also plays a role in stabilizing the thiolate anion of C22. The highest observed pK_a value was 5 (K19Q-SC-GRx), still well below the usual pK_a value (i.e., 8.4) of solvent-exposed Cys-thiols on proteins. Therefore, there must be additional mechanisms for stabilization of the C22-thiolate anion of glutaredoxin besides those contributed by K19 and C25.

Another candidate for stabilization of the C22 thiolate anion is the partial positive charge from the N-terminus of an α-helix in the vicinity of the thiolate anion. Work by Kortemme and Creighton (*36*) showed that cysteine residues at the N-terminus of an α-helix in model peptides have decreased thiol pK_a values relative to cysteine residues in unfolded model peptides. An even larger decrease in pK_a is observed when the cysteine residue is followed by a proline. This is the case for the active site region (C**P**Y/FC) of mammalian GRx1 and most of the GRx forms shown in Chart 1, except for mammalian GRx2 which displays lower catalytic activity (*37*). The proline residue is thought to lock the thiolate into a position that allows a more favorable interaction with the α-helix N-terminal partial positive charge (*36*). However, the largest decrease in pK_a observed for a cysteine-thiol attributable to stabilization by the α-helix and the succeeding proline residue in the model peptides was 1.6 pH units (*36*). Again, this interaction alone cannot account for the large decrease in the Cys22 pK_a of the glutaredoxin active site. Based on the NMR analysis, hydrogen bonding of the Cys22 thiolate with the hydroxyl

group of Thr21 may also play a role in stabilization of the active site. The close agreement between the predicted pK_a and the measured value for the natural form of GRx indicates that the physical origin of the low pK_a is captured in certain NMR deduced structures, but the essential elements are not entirely clear. Overall stabilization by a well-designed polar environment with minimal desolvation penalty, rather than a single interaction such as Lys19, is most likely involved.

CONCLUSION

According to theoretical calculations the molecular basis for stabilizing the Cys22 thiolate was predicted to relate largely to an ion-pair interaction (C22-$S^{-}\cdots{}^{+}NH_3$-K19), with some contribution from a hydrogen bond interaction involving T21. Although these calculations involve assumptions about dielectric models and conformational differences between protonated and unprotonated species that can limit the predictive power of the results, the insight on specific electrostatic interactions allows informed experimental design. According to proximity, Lys19 was identified as the major contribution to the stabilization of the Cys22 thiolate through charge−charge interaction. Hydrogen bonds with the Thr21 hydroxyl group and polar interaction with the juxtaposed α-helix may also contribute to stabilization of the thiolate anion. In addition, the entire structure surrounding Cys22 influences the magnitude of the energetic penalty for desolvation. Together these factors contribute to charge stabilization of Cys22 thiolate leading to the altered pK_a of Cys22. K19L and K19Q mutants of glutaredoxin were predicted to retain glutathionyl specificity but to lose catalytic activity due to higher pK_a values for their C22-thiol moieties. However, single site mutagenesis provides only a limited capability toward probing the physical basis underlying altered pK_a values when a structural framework is involved in generating the surrounding electrostatic environment. Nevertheless, empirical data agree qualitatively with the predictions; but the pK_a values for the mutants were increased by less than 1 pH unit, indicating that the K19 interaction is not the only contributing factor to the low pK_a of the C22-thiol. In all cases mutation of K19 did diminish catalytic activity indicating its critical contribution to catalytic turnover, an interesting outcome of the computational and empirical experiments. In the larger picture, this study has emphasized that 3-D structure elucidation and molecular modeling are valuable for developing specific mechanistic hypotheses to be tested by complementary mutational studies, although not all factors identified computationally are amenable to probing experimentally by mutagenesis.

ACKNOWLEDGMENT

The statistical mechanical method for calculating pK_a values was executed with a program generously provided by A. Yang and B. Honig (unpublished).

REFERENCES

1. Chai, Y. C., Ashraf, S. S., Rokutan, K., Johnston, R. B., and Thomas, J. A. (1994) S-thiolation of individual human neutrophil proteins including actin by stimulation of the respiratory burst: evidence against a role for glutathione disulfide, *Arch. Biochem. Biophys. 310*, 264−272.
2. Vogt, B. A., Alam, J., Croatt, A. J., Vercellotti, G. M., and Nath, K. A. (1995) Acquired resistance to acute oxidative stress. Possible role of heme oxygenase and ferritin, *Lab. Invest. 72*, 474−483.
3. Rokutan, K., Thomas, J. A., and Johnston, R. B. (1991) Phagocytosis and stimulation of the respiratory burst by phorbol diester initiate S-thiolation of specific proteins in macrophages, *J. Immunol. 147*, 260−264.
4. Rokutan, K., Johnston, R. B., and Kawai, K. (1994) Oxidative stress induces S-thiolation of specific proteins in cultured gastric mucosal cells, *Am J. Physiol. 266* (2 Part 1), G247−G254.
5. Thomas, J. A., Poland, B., and Honzatko, R. (1995) Protein sulfhydryls and their role in the antioxidant function of protein S-thiolation, *Arch. Biochem. Biophys. 319*, 1−9.
6. Mieyal, J. J., Gravina, S. A., A, M. P., Srinivasan, U., and Starke, D. W. (1995) Glutathionyl specificity of thioltransferases: mechanistic and physiological implications, in *Biothiols in health and disease* (Packer, L., and Cadenas, E., Eds.), pp 305−372, Marcel Decker, Inc., New York.
7. Cotgreave, I. A., and Gerdes, R. G. (1998) Recent Trends in Glutathione Biochemistry-Glutathione-Protein Interactions: A Molecular Link between Oxidative Stress and Cell Proliferation?, *Biochem. Biophys. Res. Commun. 242*, 1−9.
8. Klatt, P., and Lamas, S. (2000) Regulation of protein function by S-glutathiolation in response to oxidative and nitrosative stress, *Eur. J. Biochem. 267*, 4928−4944.
9. Shelton, M. D., Chock, P. B., and Mieyal, J. J. (2005) Glutaredoxin: Role in Reversible Protein S-Glutathionylation and Regulation of Redox Signal Transduction and Protein Translocation. *Antioxid. Redox Signaling 7*, 348−366.
10. Bandyopadhyay, S., Starke, D. W., Mieyal, J. J., and Gronostajski, R. M. (1998) Thioltransferase (Glutaredoxin) Reactivates the DNA-binding Activity of Oxidation-inactivated Nuclear Factor I, *J. Biol. Chem. 273*, 392−397.
11. Davis, D. A., Newcomb, F. M., Starke, D. W., Mieyal, J. J., and Yarchoan, R. (1997) Thioltransferase (Glutaredoxin) Is Detected Within HIV-1 and Can Regulate the Activity of Glutathionylated HIV-1 Protease *in Vitro*, *J. Biol. Chem. 272*, 25935−25940.
12. Barrett, W. C., DeGnore, J. P., Konig, S., Fales, H. M., Keng, Y.-F., Zhang, Z.-Y., Yim, M. B., and Chock, P. B. (1999) Regulation of PTP1B via glutathionylation of the active site cysteine 215, *Biochemistry 38*, 6699−6705.
13. Gravina, S. A., and Mieyal, J. J. (1993) Thioltransferase is a specific glutathionyl mixed disulfide oxidoreductase, *Biochemistry 32*, 3368.
14. Yang, Y., Jao, S.-C., Nanduri, S., Starke, D. W., Mieyal, J. J., and Qin, J. (1998) Reactivity of the human thioltransferase (glutaredoxin) C7S, C25S, C78S, C82S mutant and NMR solution structure of its glutathionyl mixed disulfide intermediate reflect catalytic specificity, *Biochemistry 37*, 17145−17156.
15. Chrestensen, C. A., Starke, D. W., and Mieyal, J. J. (2000) Acute cadmium exposure inactivates thioltransferase (glutaredoxin), inhibits intracellular reduction of protein-glutathionyl-mixed disulfides, and initiates apoptosis, *J. Biol. Chem. 275*, 26556−26565.
16. Fernandes, A. P., and Holmgren, A (2004) Glutaredoxins: glutathione-dependent redox enzymes with functions far beyond a simple thioredoxin backup system, *Antioxid. Redox Signaling 1*, 63−74.
17. Yang, Y., and Wells, W. W. (1991) Identification and characterization of the functional amino acids at the active center of pig liver thioltransferase by site-directed mutagenesis, *J. Biol. Chem. 266*, 12759−12765.
18. Srinivasan, U., Mieyal, P. A., and Mieyal, J. J. (1997) pH profiles indicative of rate-limiting nucleophilic displacement in thioltransferase catalysis, *Biochemistry 36*, 3199−3206.
19. Srinivasan, U. (1998) Mechanism of Catalysis and Inactivation of Thioltransferase, Ph.D. Thesis, Case Western Reserve University (Mieyal, J. J., Advisor).
20. Mieyal, J. J., Starke, D. W., Gravina, S. A., and Hocevar, B. (1991) Thioltransferase in Human Red Blood Cells: Kinetics and Equilibrium, *Biochemistry 30*, 8883−8891.
21. Gan, Z. R., Polokoff, M. A., Jacobs, J. W., and Sardana, M. K. (1990) Complete amino acid sequence of yeast thioltransferase (glutaredoxin), *Arch. Biochem. Biophys. 282*, 110−115.
22. Sun, C., Berardi, M. J., and Bushweller, J. H. (1998) The NMR Solution Structure of Human Glutaredoxin in the Fully Reduced Form, *J. Mol. Biol. 280*, 687−701.
23. Yang, A.-S., Gunner, M. R., Sampogna, R., Sharp, K., and Honig, B. (1993) On the calculation of pKas in proteins, *Proteins: Struct., Funct., Genet. 15*, 252−265.
24. Warwicker, J., and Gane, P. J. (1996) Calculation of Cys 30 delta pKa's and oxidising power for DsbA mutants, *FEBS Lett. 385*, 105−108.

25. Dillet, V., Dyson, H. J., and Bashford, D. (1998) Calculations of Electrostatic Interactions and p*K*as in the Active Site of *Escherichia coli* Thioredoxin, *Biochemistry 37*, 10298−10306.
26. Beroza, P., Fredkin, D. R., Okamura, M. Y., and Feher, G. (1991). Protonation of interacting residues in a protein by a Monte Carlo method: application to lysozyme and the photosynthetic reaction center of Rhodobacter sphaeroides, *Proc. Natl. Acad. Sci. U.S.A. 88*, 2233−2250.
27. Nicholls, A., and Honig, B. (1991) A rapid finite difference algorithm, utilizing successive over-relaxation to solve the Poisson-Boltzmann equation, *J. Comput. Chem. 12*, 435−445.
28. Rocchia,W., Alexov, E., and Honig, B. (2001) Extending the Applicability of the Nonlinear Poisson-Boltzmann Equation: Multiple Dielectric Constants and Multivalent Ions, *J. Phys. Chem. B 105*, 6507−6514.
29. MacKerell, J. A. D., Bashford, D., Bellott, M., Dunbrack, R. L., Jr., Evanseck, J., Field, M. J., Fischer, S., Gao, J., Guo, H., Ha, S., Joseph, D., Kuchnir, L., Kuczera, K., Lau, F. T. K., Mattos, C., Michnick, S., Ngo, T., Nguyen, D. T., Prodhom, B., Reiher, I., W. E., Roux, B., Schlenkrich, M., Smith, J., Stote, R., Straub, J., Watanabe, M., Wiorkiewicz-Kuczera, J., Yin, D., and Karplus, M. (1998) All-Atom Empirical Potential for Molecular Modeling and Dynamics Studies of Proteins, *J. Phys. Chem. B 102*, 3586−3616.
30. Dominy, B. N., and Brooks, C. L., III (2002) Identifying native-like protein structures using physics-based potentials, *J. Comput. Chem. 23*, 147−160.
31. Szajewski, R. P., and Whitesides, G. M. (1980) Rate constants and equilibrium constants for thiol-disulfide interchange reactions involving oxidized glutathione, *J. Am. Chem. Soc. 102*, 2011−2026.
32. Gilbert, H. F. (1990) Molecular and cellular aspects of thiol-disulfide exchange. *Adv. Enzymol. Relat. Areas Mol. Biol. 63*, 69−172.
33. Gustafsson, A., Pettersson, P. L., Grehn, L., Jemth, P., and Mannervik, B. (2001) Role of the glutamyl alphacarboxylate of the substrate glutathione in the catalytic mechanism of human glutathione transferase A1-1. *Biochemistry 40*, 15835−15845.
34. Allardyce, C. S., McDonagh, P. D., Lian, L.-.Y, Wolf, C. R., and Roberts, G. C. K. (1999) The role of tyrosine-9 and the C-terminal helix in the catalytic mechanism of Alpha-class glutathione S-transferases. *Biochem. J. 343*, 525−531.
35. Jao, S.-C. (1999) Mutagenic, NMR, and Molecular Modeling Studies of Thioltransferase, Ph.D. Thesis, Case Western Reserve University (Mieyal, J. J., and Post, C. B., Advisors).
36. Kortemme, T., and Creighton, T. E. (1995) Ionisation of cysteine residues at the termini of model alpha-helical peptides. Relevance to unusual thiol pK_a values in proteins of the thioredoxin family. *J. Mol. Biol. 253*, 799−812.
37. Johansson, C., Lillig, C. H., and Holmgren, A. (2004) Human mitochondrial glutaredoxin reduces S-glutathionylated proteins with high affinity accepting electrons from either glutathione or thioredoxin reductase, *J. Biol. Chem. 279*, 7537−7543.
38. Thompson, J. D., Plewniak, F., Thierry, J., and Poch, O. (2000) DbClustal: rapid and reliable global multiple alignments of protein sequences detected by database searches, *Nucleic Acids Res. 28*, 2919−2926.

BI0516327